Applied Surface Science 443 (2018) 167–175

Contents lists available at ScienceDirect

Applied Surface Science

journal homepage: www.elsevier.com/locate/apsusc

Full Length Article

Effects of laser polishing on surface microstructure and corrosion resistance of additive manufactured CoCr alloys

W.J. Wang *, K.C. Yung, H.S. Choy, T.Y. Xiao, Z.X. Cai

Department of Industrial and Systems Engineering, The Hong Kong Polytechnic University, Hung Hom, Kowloon, Hong Kong

ARTICLE INFO

Article history:
Received 15 December 2017
Revised 22 February 2018
Accepted 24 February 2018
Available online 3 March 2018

Keywords:
CoCr alloy
Laser polishing
Corrosion resistance
Additive manufacturing
Crystalline structure

ABSTRACT

Laser polishing of 3D printed metal components has drawn great interest in view of its potential applications in the dental implant industries. In this study, corrosion resistance, surface composition and crystalline structure of CoCr alloys were investigated. The corrosion resistance, micromorphology, composition, phase transformations and crystalline structures of samples were characterized using an electrochemical analyzer, scanning electron microscope (SEM), energy dispersive X-ray spectroscopy (EDX), X-ray diffraction (XRD) and transmission electron microscope (TEM), respectively. The results indicate that high laser powers and low object distances within a certain range can facilitate the formation of complex oxide films, which exhibits high corrosion resistance. Further, object distances have a significant influence on cooling rates during the solidification of the melt pool in laser polishing, and fast cooling generates vast amounts of vacancies and defects, which result in the crystalline phase transformation from γ to ε. Consequently, the formed oxides play an important role in corrosion resistance on the outer layer, and inner layer with γ phase also helps keep the CoCr alloys in a stable structure with high resistant to corrosion. The two process parameters in laser polishing, laser power and object distances, are demonstrated as being important for controlling the surface microstructures and corrosion resistance of the additive manufactured CoCr alloy components.

1. Introduction

CoCr alloys have been widely used in dentistry for dentures or artificial prostheses for replacement of missing dental tissues including teeth, bone, retainer and baseplate [1]. However, the continuous release of metal ions from metal implants in the oral environment possibly causes a toxicity problem with body fluids [2]. Due to the potential risks of CoCr alloys being applied in the human body, many studies [3–8] have focused on the corrosion resistance of cast Co—Cr—Mo alloys, considering the composition, electrolyte solutions and structures etc. Corrosion resistance of Co—Cr—Mo alloys, with varying content of elements and additives, was also studies in different biological solutions such as urine, joint fluid, serum, saline solution, Hanks and cell culture media. The elemental content exhibited was found to have a more significant effect than the electrolyte solutions [9,10]. Basically, both the elemental content of Co—Cr—Mo alloys and the preparation processes have great influence on the microstructures and phases due to different interfacial properties [11–14]. Generally, the more stable the oxide film formed in Co—Cr—Mo implant alloy, the better is the corrosion resistance. The release of metallic ions from implant alloy is also much less [9].

Currently, additive manufacturing has drawn great attention for its potential applications in the dental implant industries [15–17] to replace the conventionally cast Co-Cr-Mo alloys. This can eliminate the time-consuming casting process, produce consistent quality and better dimensional accuracy of less than 40 μm [18]. Recent studies have focused on surface modification using lasers to outcome the limitations in the existing polishing methods on the inner structures of the 3D printed components, which need to satisfy strict surface requirements in medical applications [19,20]. Actually, the resolution range of the 3D printed metal components leads to a rough surface larger than 5 μm, which has great influence on corrosion resistance. However, the surface microstructure and corrosion resistance of laser polished additive manufactured CoCr alloys has not been thoroughly investigated.

In this work, the effect of laser polishing on the surface microstructure and corrosion resistance of additive manufactured CoCr alloy components was investigated. The corrosion behavior of additive manufactured CoCr alloys before and after laser polishing were characterized. In addition, surface composition, crystalline structure and corrosion mechanisms were also evaluated and discussed.

* Corresponding author.
E-mail address: wendy.wang@polyu.edu.hk (W.J. Wang).

https://doi.org/10.1016/j.apsusc.2018.02.246
0169-4332/

2. Materials and experimental

2.1. Materials and preparation

Additive manufactured components made of CoCr alloys were printed in a rectangular slab with dimensions of 100 × 75 × 8 mm^3 by a SLM 125 HL 3D Printer, with 400 W power and argon gas under an inert environment. CoCr/2.4979/F75 powder was used, with chemical composition, as shown in Table 1. The surface layer of the metal sample was combined into several layers of powder, with a slice thickness of 0.025 mm, using the laser melting process. The direction of the printed lines in each layer was perpendicular to each other. The scanning velocity of the laser beam was about 450 mm/s.

A 70 W fiber laser was used for polishing the 3D printed CoCr. The laser beam of this pulsed fiber laser was initiated by a 70 W 1065 nm laser source, which was produced by the SPI Laser, with the beam expander collimator of model F75 BEC.

Table 1
Composition of 3d printing powder of cobalt-chromium (CoCr).

Composition (wt.%)	Cobalt-chromium alloy (CoCr)(%)
Co	60.00–68.00
Cr	27.00–30.00
Al	<0.01
B	<0.01
C	<0.01
Fe	<0.75
Mn	<1.00
Mo	5.00–7.00
N	<0.25
Ni	<0.50
P	<0.02
S	<0.01
Si	<1.00
Ti	<0.10
W	<0.20

Based on a previous study, the laser power and object distance (defined as the height difference between the laser lens and the surface of the metal sample) have a remarkable effect on the surface roughness and wettability of laser polished CoCr, and also a great influence on the corrosion resistance of laser polished CoCr. The surface roughness of the unpolished additive manufactured CoCr was about 5 μm, and that of the optimal laser polished CoCr was about 0.45 μm, as shown in Fig. 1. Besides, the surface roughness of the CoCr samples decreased rapidly from 4.976 μm to 0.45 μm as the percentage of laser power increases from 40% to 100%, and that of the CoCr samples sharply increases from 0.45 μm to 15.91 μm as the object distances increases from 204 mm to 208 mm. Rougher surfaces have higher surface energy, so a surface in more unstable state is easy to become defective and corroded [21]. Accordingly, samples with different laser power percentages of 40% and 100% and with different object distances of 204 mm, 206 mm and 208 mm were used for a study of corrosion resistance. As the focusing distance (the height between the laser lens and focus position for the metal sample) was fixed at an object distance of 210 mm, object distances that deviated from the focusing distance could also be viewed as defocusing distances.

All the experiments were carried out at ambient temperature (298–303 K), and conducted as in the simple variable method given in Table 2.

2.2. Characterization methods

Surface micromorphology was carried out using a JEOL Model JSM-6490 field emission scanning electron microscope (SEM). The surface elements were analyzed by a energy dispersive X-ray spectroscopy (EDX) detector.

The surface phases of the coating samples (10 × 10 mm^2) were measured by an Empyrean (PANanalytical) X-ray diffraction system with a radiation source of Cu K ray, tube voltage of 40 kV, tube current of 40 mA, diffraction angle between 30° and 100°, and scanning speed at 1.8°/min.

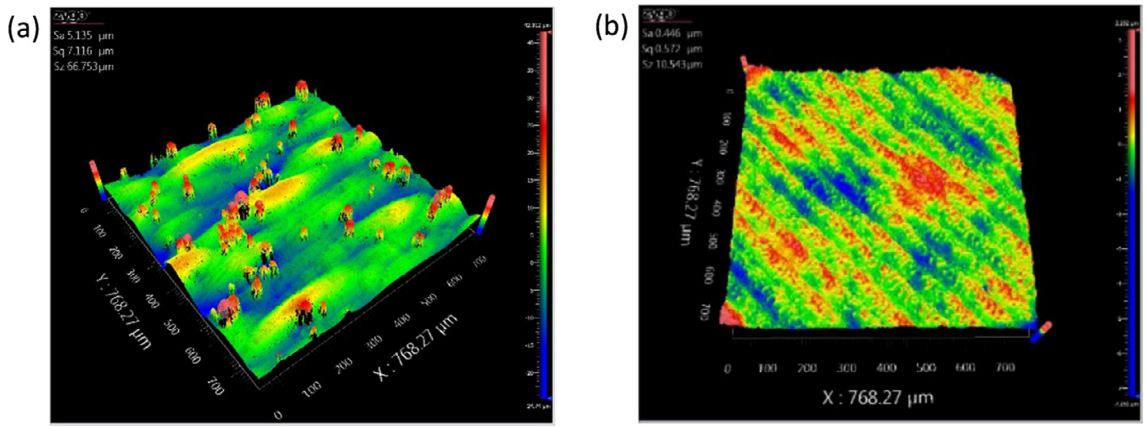

Fig. 1. Optical profile images of the unpolished (a) and optimal laser polished (b) additive manufactured CoCr alloys.

Table 2
Levels and factors of laser polishing parameters.

Sample reference	Object distances mm	Laser power percentage (%) at 70 W	Scanning velocity mm/s	Hatching space mm	Flow rate l/min
0#	No treatment				
1#	204	40	500	0.05	6
2#	206	40			
3#	208	40			
4#	204	100			
5#	206	100			
6#	208	100			

The grain structure and boundaries of the pre- and post-laser polished samples were observed by JEM 2010 (JEOL) TEM.

The corrosion resistance of the coatings was evaluated by a Princeton electrochemical analyzer. A three electrode system with the auxiliary electrode of Pt chip ($15 \times 15\ mm^2$), reference electrode of saturated calomel and working electrode of pre- and post-laser polished CoCr alloy samples ($10 \times 10\ mm^2$) was selected. Saline solution (saline, 0.9 wt.% NaCl solution) was applied. The potential dynamic polarization curve was determined over a potential range of −1.0 to 1.5 V, scan rate of 2 mV/s.

3. Results and discussion

3.1. Polarization analysis

Fig. 2 shows potential dynamic polarization curves of the pre- and post-laser polished CoCr alloys. The corrosion potential (E_c) and corrosion current density (I_c) were obtained by Tafel extrapolation. The E_c of the unpolished sample 0# was −0.36 V, and the I_c of that 0.97 μA/cm^2. The E_c values of laser polished CoCr alloys with 40% laser power and object distances varying from 204 mm to 208 mm (samples of 1#, 2# and 3#) were −0.31 V, −0.33 V and −0.49 V, while those of I_c were 0.25 μA/cm^2, 0.07 μA/cm^2 and 0.05 μA/cm^2 respectively. The Ec of laser polished CoCr alloys with 100% laser power and object distances varying from 204 mm to 208 mm (samples of 4#, 5# and 6#) were −0.22 V, −0.40 V and −0.20 V, while those of I_c were 0.11 μA/cm^2, 0.02 μA/cm^2 and 2.96 μA/cm^2, respectively. Obviously, the most outer layers of samples 4# and 6# showed the most positive potential compared to other samples (1#, 2#, 3# and 5#), which indicating the lowest activation in chemical reaction and the lowest possibility of corrosion, based on the thermodynamics of corrosion [22–24]. However, the I_c values of laser polished CoCr alloy samples were much smaller than those of the unpolished sample 0# except for sample 6#. Sample 5# shows the smallest corrosion current density compared to the other samples (1#–4# and 6#), which indicates the slowest corrosion rate and a high corrosion resistance. In consideration of both the corrosion potential and corrosion current density, it can be inferred that sample 4# has high corrosion resistance. Nyquist plots of unpolished and laser polished Co—Cr—Mo alloy are presented in Fig. 3, where sample 4# exhibits a typical passive alloy system over a relatively wide frequency region. That result clearly

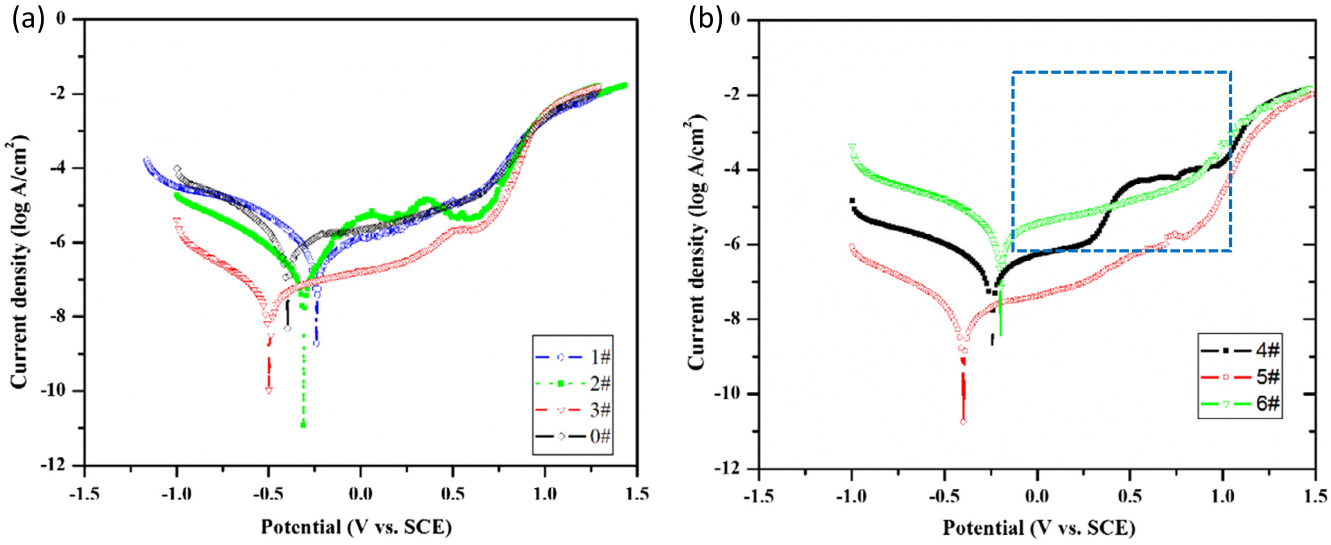

Fig. 2. Potentiodynamic polarization curves of the pre- and post-laser polished CoCr alloys.

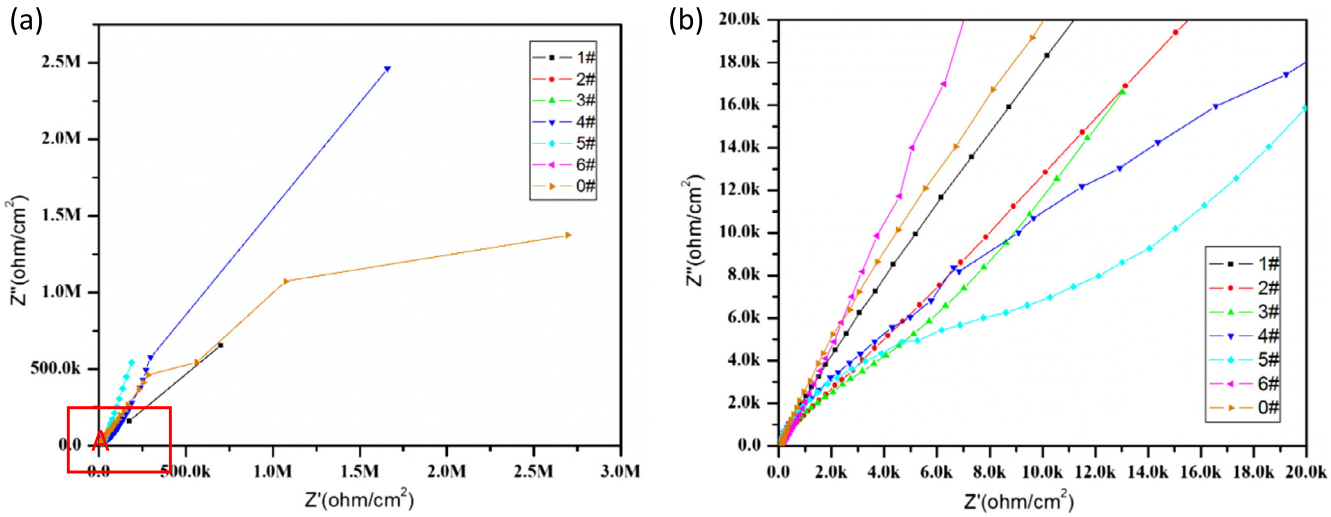

Fig. 3. Nyquist impedance spectra of the pre- and post-laser polished CoCr alloys (a) and their partial enlarged images at Zone A of b.

demonstrates the large polarization resistance and high corrosion resistance for sample 4#. Compared with the corrosion resistance (E_c with −0.3 V) reported in previous works for CoCr alloys with thermo mechanical treatment, such as casting, annealing, ultrasonic and hot forging, our tested samples (E_c with −0.22 V) are appreciably ~30% better while under similar corrosion conditions in a saline solution [10,13].

Sample 4# shows very different passivity regions from the other samples (1#–3#, 5# and 6#). It can be seen that the laser polished CoCr alloy with 100% laser power and an object distance of 204 mm has two passivity regions on the anodic branch of potential dynamic polarization curve, as shown zone A in Fig. 2b, at potentials of −0.14 V to 0.28 V and 0.48 V to 1.0 V. The other samples (1#–3#, 5# and 6#) have only one passivity region and they are

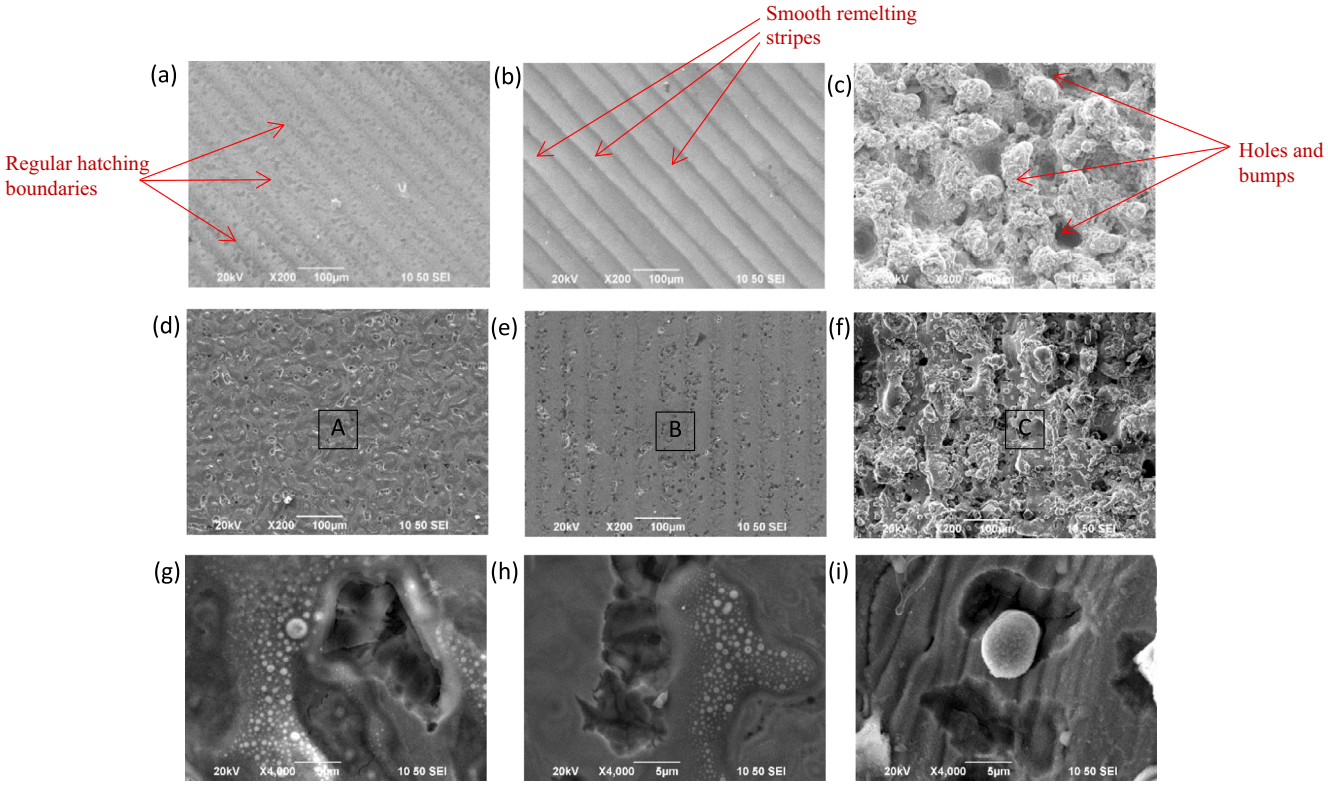

Fig. 4. SEM images of uncorroded (a 204 mm, b 206 mm, c 208 mm) and corroded (d 204 mm, e 206 mm, f 208 mm, and their partial enlarged images at Zone A of d, at Zone B of e, and at Zone C of f are shown in g 204 mm, h 206 mm and i 208 mm respectively) surfaces of the laser polished CoCr alloys with 100% laser power and different defocusing distances.

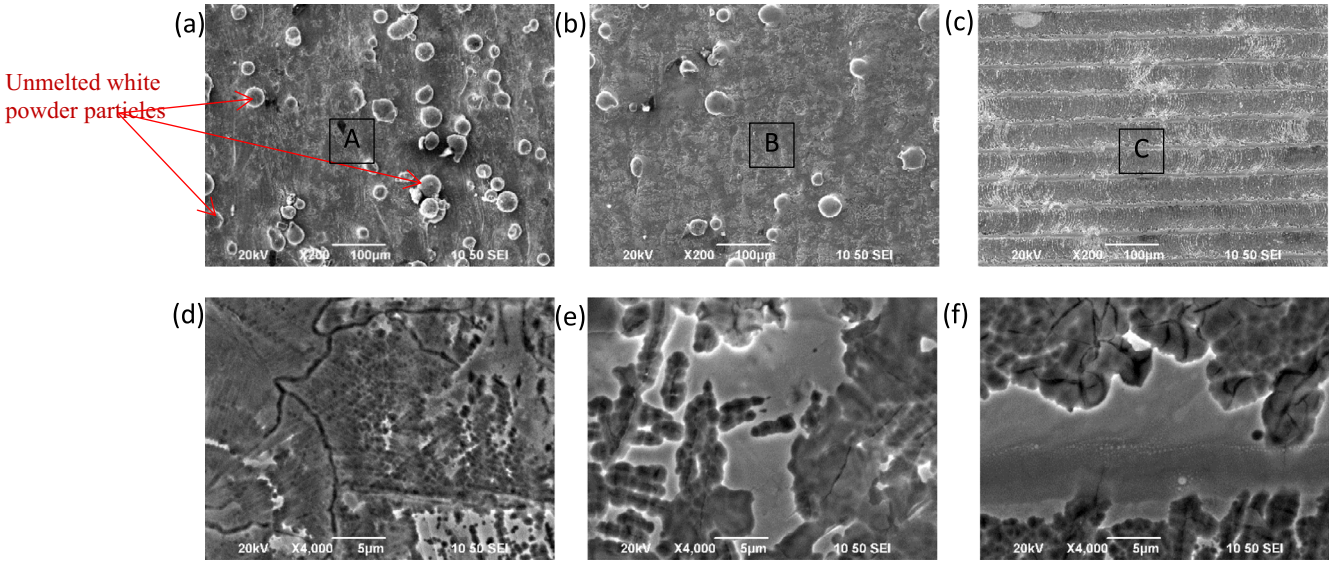

Fig. 5. SEM images of corroded (a 204 mm, b 206 mm, c 208 mm, and their partial enlarged images at Zone A of d, at Zone B of e, and at Zone C of f are shown in d 204 mm, e 206 mm and f 208 mm respectively) surfaces of the laser polished CoCr alloys with 40% laser power and different defocusing distances.

varying at potentials from −0.4 V to 1.0 V. This behavior strongly suggests at the formation of a passive film and a breakdown of the formed passive film. As the sample surface was immersed in saline solution, the oxide film passed through dissolution/depassivation and growth/repassivation processes [25]. However, the results also correlate with the structures and phases of the inner and outer layers as well.

Fig. 4 shows the surface micromorphology of the uncorroded and corroded surfaces of laser polished CoCr with 100% laser power and different defocusing distances. It is clearly seen that pitting corrosion at the hatching boundaries formed due to the laser scanned paths, with pitting sizes differing with the varied process parameters in the laser polishing. Based on the EDX results, the amounts of oxide at regular hatching boundaries and smooth remelting stripes, as shown in Fig. 4a and b, are different. The different oxides can cause a high chance of pitting corrosion at the hatching boundaries while the stripes inhibit corrosion. However, Fig. 4c shows a great number of large holes and bumps, whose appearance gives difficulties in facilitating the formation of an integrated oxide film to protect the inner layer. The surfaces can thus be severely corroded, leading to exposure of the inner 3D printing layer structures, as shown in Fig. 4i.

In comparison, laser polished CoCr alloys with 40% laser power and different object distances, as in Fig. 5, show a very different corroded surface micromorphology from that of with 100% laser power. Due to the lower laser power, there are still many unmelted white powder particles on the surface and the whole surface is almost corroded because of the incomplete oxide films. Pitting corrosion is observed in the partial enlarged images shown in Fig. 5d–e. This is because the low laser power cannot supply sufficient energy for the formation of dense oxide films with the required thickness, which results in surface defects not covering the complete oxide film. Besides, cracks or grain boundaries are clearly detected, probably be generated by stress concentrations, and are more likely to be corroded.

3.2. Crystalline structure

XRD patterns of the pre- and post-laser polished CoCr alloys are shown in Fig. 6. The untreated CoCr alloy shows γ and ε crystalline phases, while the intensity of γ structure is much stronger than that of ε. Basically, no matter whether a high laser power (100%) or low laser power (40%) is used, with increase of the object distance, the intensity of the γ phase is increased gradually and that of ε phase is inversely decreased. Besides, with the increase of the object distance, the amounts and kinds of oxides are decreased at high laser power. On the contrary, the extent of the oxides is accordingly increased at low power. The peaks at 2θ are 44.30°, 51.55° and 76.05°, corresponding to (1 1 1)γ, (2 0 0)γ and (2 2 0)γ planes. Further, the XRD pattern indicates that the sample is free from any oxides or carbides, as shown in Fig. 5a–c. However, the ε phase of laser treated CoCr at 40% laser power becomes faded and the γ phase becomes strong and clear. The major constituents of laser polished CoCr alloy at 40% laser power and object distances varying from 204 mm to 208 mm have similar γ and ε phases. The varying intensity of the γ phase shows that the amount of γ phase increases with the decreasing gap between the object distance and focus. Moreover, the increasing intensity of the γ phase corresponds to increasing FWHM (full width at half maximum).

Eq. (1), the Debye-Scherer equation can be used for calculating the crystal size. 2θ is the most intensive peak, which refers to the (111) crystal face, and FWHM (β) was transferred to radiation. Cu target Kα radiation was employed, while Kα (1.5431 Å) radiation was composed of Kα1 (1.5406 Å) and Kα2 (1.5443 Å) at a ratio of 0.5. Accordingly, the three crystal sizes of laser polished CoCr alloys at 40% laser power and object distances varying from 204 mm to 208 mm are 29.2 nm, 29.0 nm and 24.2 nm, respectively. Obviously, the different grain sizes formed are the result of different nuclear energies, supplied by the laser source due to the varying object distances. Laser polished CoCr alloys at 100% laser power and object distances varying from 204 mm to 208 mm have a similar influence on the change of grain sizes, which are 29.1 nm, 24.2 nm and 24.1 nm, respectively.

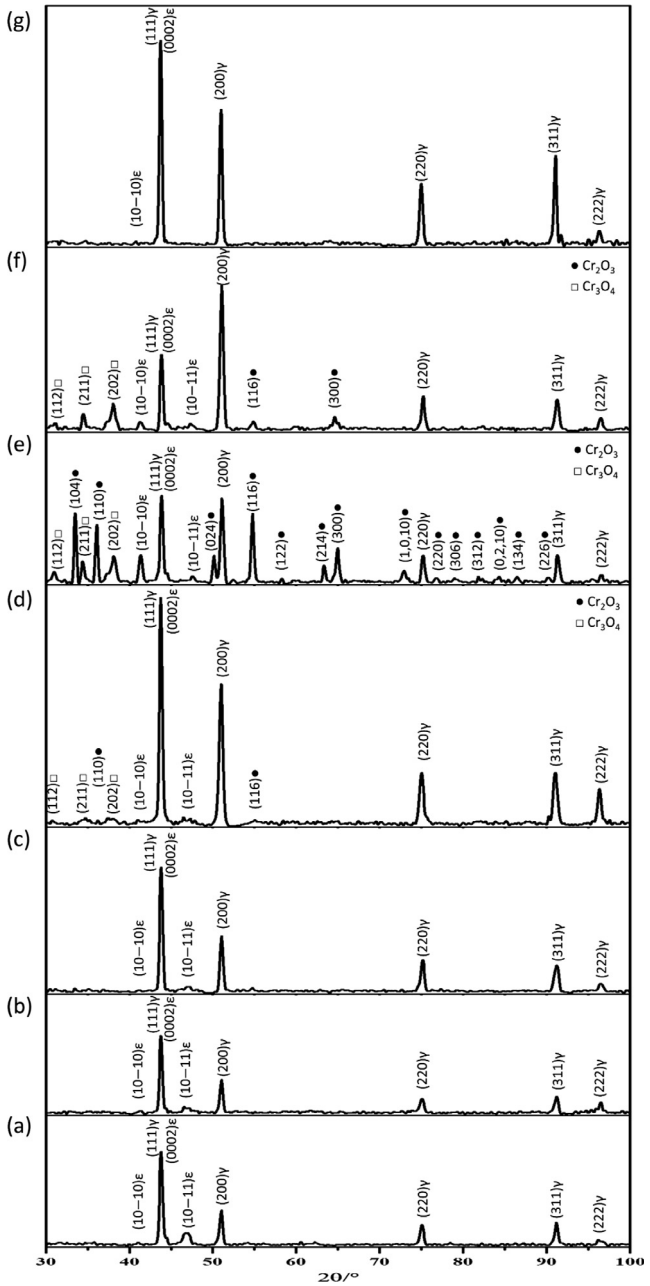

Fig. 6. XRD patterns for the unpolished (a) and laser polished (b 40% 204 mm, c 40% 206 mm, d 40% 208 mm, e 100% 204 mm, f 100% 206 mm, g 100% 208 mm) CoCr alloys.

$$D = \frac{0.9\lambda}{\beta \cos\theta} \quad (1)$$

where D is the crystal size, λ is the wave length of Kα radiation, β is the full width at half maximum (FWHM) and 2θ is the radiation angle.

With the increased laser power, the grains are refined, which is disadvantageous in improving corrosion resistance. Due to the grain refinement under a mono phase state or alloying, the grain interfaces are added, which most likely results in lower corrosion resistance, such as in sample 6#. However, if the grain refinement is accompanied with improved interfacial structures, corrosion resistance can be enhanced. Naturally, the shapes of the grain boundaries have a great influence on corrosion resistance, which can be improved by a low energy interface or by forming a densely passive film.

Therefore, in Fig. 6d–f, there are different kinds of oxides obtained. The main peaks at 2θ are 31.25°, 34.74° and 37.60° corresponding to the (1 1 2), (2 1 1) and (2 0 2) planes of the Cr_3O_4 phase and those at 2θ are 33.60°, 36.19° and 54.85° corresponding to (1 0 4), (1 1 0) and (1 1 6) planes of the Cr_2O_3. In the XRD patterns of samples 4# to 6# (Fig. 6e–g), the intensity of the oxide peaks becomes faded, which indicates that the oxides are hard to form as the object distance is increased. However, in samples 1# to 3# (Fig. 6b–d), the intensities of the oxide peaks are prominent, which means that the low laser power supplied is not enough to provide the required nuclear energy for metal atoms to bond with oxygen. Due to the formation of a passive film containing chromium oxides, the CoCr alloys show high corrosion resistance. The elemental composition, microstructure and thickness of passive oxide film are changed with the process parameters in laser polishing. Consequently, the XRD results show main phases are the Co matrix with Cr oxides. Thus, although samples 1# and 2# have large grain sizes (which may lead to high corrosion resistance), they are still easily corroded, which results from insufficient or no oxides (based on Fig. 6b and c) to protect the CoCr alloy surfaces.

The standard electrode potentials of Cr^{3+} and Cr^{2+} are shown below:

$$Cr^{3+} + e^- \rightarrow Cr^{2+} \quad \varphi^\theta = -0.41\ V \tag{2}$$

$$Cr^{3+} + 3e^- \rightarrow Cr \quad \varphi^\theta = -0.74\ V \tag{3}$$

$$Cr^{2+} + 2e^- \rightarrow Cr \quad \varphi^\theta = -0.91\ V \tag{4}$$

The oxide Cr_3O_4 is considered as a mixture of Cr_2O_3 and CrO, in the presence of Cr^{3+} and Cr^{2+}. In the electrochemical test, the reaction is in the reduction of Cr^{3+} and Cr^{2+}. Obviously, the most negative potential shown in Eq. (4) is the first possible reaction, which means the oxide film of Cr_3O_4 is broken firstly, then the Cr_2O_3 film follows. Consequently, sample 4# has large amounts of Cr oxides, and two passive steps and high corrosion resistance are observed, while the other samples (1#–3#, 5# and 6#) only have one passive step observed.

The above conclusions are further verified by TEM observations, as described in next section.

3.3. TEM analysis

Fig. 7 is an SEM micrograph of a corroded surface of CoCr alloy. Cellular structures with visible spaces of the ε phase are readily observed, and the ε phase is accompanied with more defects, such as cracks, holes and voids, which are more likely to be corroded. Based on previous work in casting, the annealing temperature and cooling rate have great influence on γ and ε crystalline phase transformation, and rapid solidification results in the formation of vacancies and planar defects (stacking faults), promoting γ to ε transformation [26–28]. Obviously, with the increase of object distance, the gap between object surface and laser focus distance is decreased, which leads to a decreased cooling rate during the solidification of the melting pool in laser polishing, and phase transformation from γ to ε. Further, 3D printing components with selective laser melting (SLM) technology have both heating and rapid cooling steps in the additive manufacturing process, which means the γ phase is obtained when the layer is formed and is transformed from γ phase to ε phase during consolidation when heating and building next layer. Similar findings for unpolished 3D CoCr alloy with major γ phase and ε trace phase have been reported [16,29]. Therefore, the surface of laser polished CoCr alloy appears to have the inner structure of unpolished CoCr alloy including γ phase and ε phase, which undergoes reheating and phase transformation [30,31].

The corresponding TEM results are shown in Fig. 8, which confirms that the matrix is composed of a solid solution of chromium in cobalt, with stacking faults and defects. The (1 1 1) and (3 1 1) planes of the γ phase have satellites along the direction of the ⟨1 −1 −2⟩ lattice axis, and the (0 0 0 2) and (1 1 −2 2) planes of the ε phase have satellites along the directions of the ⟨1 −1 0 0⟩ lattice axis. They are parallel in the ε and γ phase. The (0 0 0 2) planes of the ε phase and the (1 1 1) planes of the γ phase, with orientation parallel to the sample surface, can be readily nucleated for the growth of durable and stable oxides, and the hexagonal close packed (hcp) structure can enhance corrosion resistance [32–34]. As shown in Figs. 9 and 10, oxides of the laser polished CoCr alloys are detected. Cr_3O_4 with a tetragonal structure shows (1 1 2) and (2 2 0) planes growing along with the ⟨1 −1 0⟩ lattice

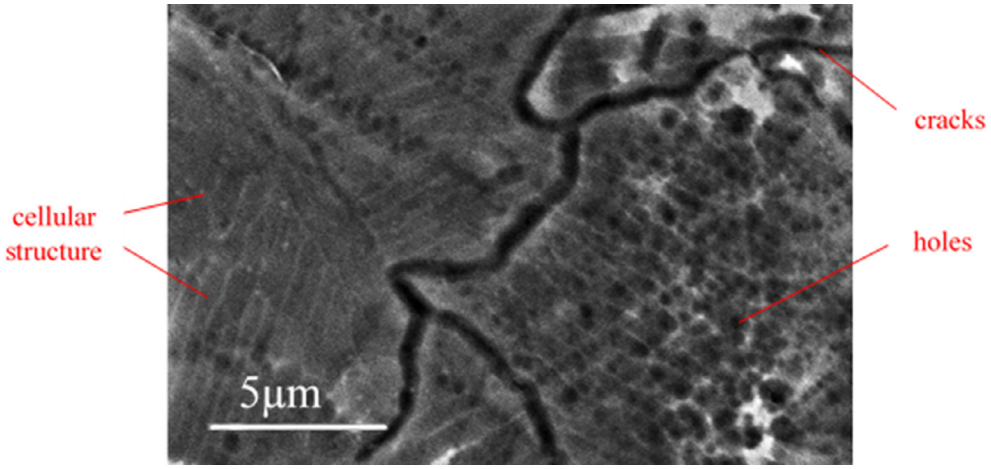

Fig. 7. SEM image of cellular structure of the corroded CoCr alloys.

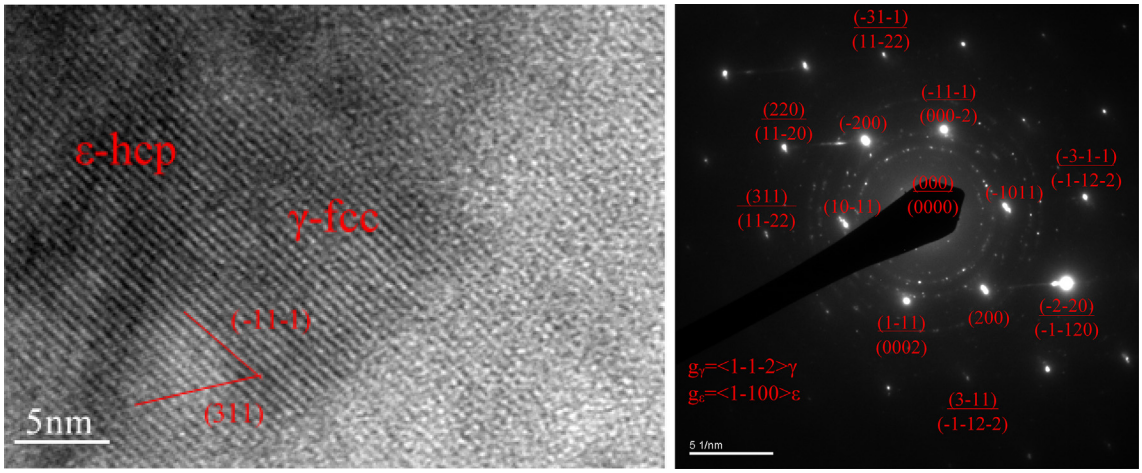

Fig. 8. HRTEM image of CoCr alloy surface and its corresponding electron diffraction pattern.

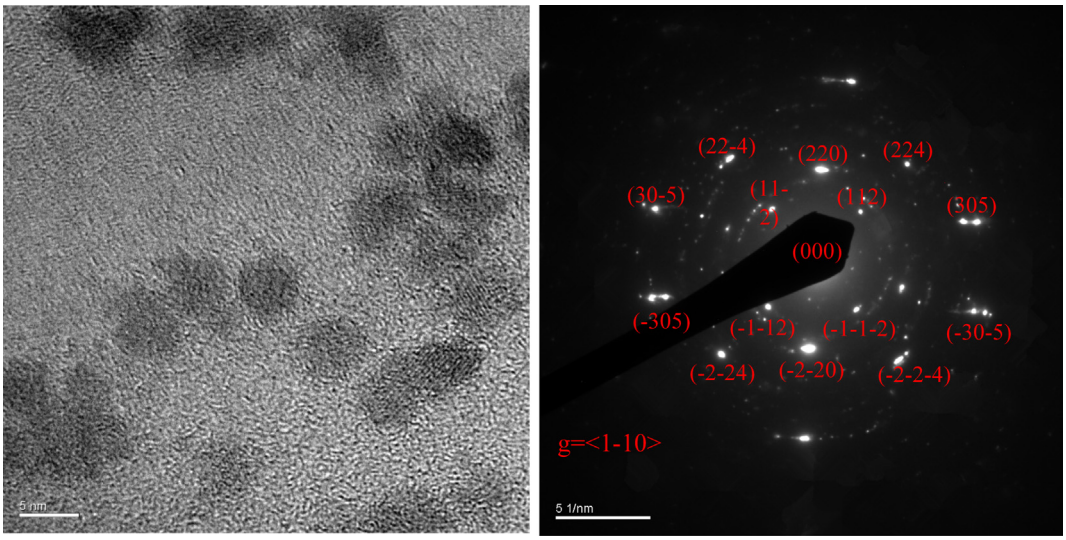

Fig. 9. HRTEM image of Cr_3O_4 in CoCr alloy surface and its corresponding electron diffraction pattern.

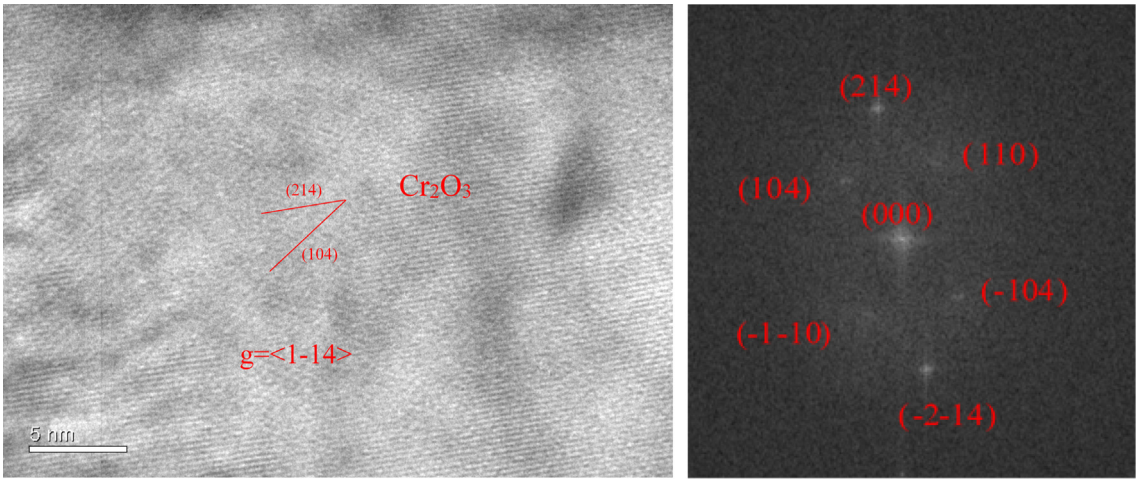

Fig. 10. HRTEM image of Cr_2O_3 in CoCr alloy surface and its corresponding electron diffraction pattern.

axis, while Cr_2O_3 with a hexagonal structure shows (1 1 0) and (1 0 4) planes growing with the ⟨1 −1 4⟩ lattice axis. It is clearly indicated that both Cr_3O_4 and Cr_2O_3 have the parallel growth directions with the ε phase.

It is noteworthy that an inherent stacking fault on the (1 1 1) crystallographic plane in face centered cubic (fcc) can generate an hcp stacking sequence, which may lead to a few narrow plates of the residual planes of the fcc stacking sequence in the hcp

regions. Besides, the transformation in metals is most probably accompanied with a high vacancy in the hcp region for the vacancy formation energy, which appears as if the hcp "equilibrates" or "recrystallizes" simultaneously with precipitate coarsening [27,35].

Due to increasing corrosion resistance with the oxides of outer layer and decreasing corrosion resistance with the hcp structure and transformation from γ to ε of subsurface or inner layer, all test samples are not completely consistent at the initial corrosion potential and corrosion current density. For instance, sample 4# shows positive corrosion potential (Fig. 2b) with the amount of oxides (Fig. 6e) in outer layer and slightly fast (compared with the slowest) corrosion current density with increased hcp structure and ε phase in the subsurface or inner layer (Figs. 6e and 8). Therefore, chromium oxide appears to be the most resistant to dissolution at the first moments of immersion. However, the transformations are related to the structure and phase that promotes a stable oxide film and advanced structural state in the surface layer.

Thus, it is evident that laser polishing can effectively improve the surface microstructure and corrosion resistance of additive manufactured components. This is attributed to the microstructural control in attaining equilibrium between the hcp structure and oxides. This phenomenon makes it possible to design a CoCr alloy with an anticorrosion protective layer and with unique properties for odontological applications [36], such as dental bridges and dentures to be used in an oral environment. Also, the surface microstructure in CoCr alloys by laser polishing is smooth and this can enhance the resistance of bacterial plaque accumulation.

4. Conclusions

This work studies the effect of laser polishing on the surface microstructure and corrosion resistance of additive manufactured CoCr alloy components. The following conclusions can be drawn from the results:

(1) In consideration of both the corrosion potential and corrosion current density, laser polished samples are found to have higher corrosion resistance and are about 30% better than some thermo mechanical treatment samples reported in previous studies.
(2) The oxides on the outer layer and structures in the inner layer play important roles in the corrosion resistance of laser polished samples, and the most important process parameters for laser polishing process are laser power and object distance.
(3) The difficulty of oxide growth is influenced by the directions of the ε phase, and the crystalline phase transformation from γ phase to ε phase is accompanied with vacancies and planar defects.

These results indicate that laser polishing can improve the surface microstructure and corrosion resistance of additive manufactured CoCr alloy components by effectively controlling the hexagonal close packed structures and the formed oxides. Laser polished CoCr alloy components, with improved corrosion resistance, are attractive for potential applications as dental implants in prosthodontics.

Acknowledgement

This work was funded by the Hong Kong Innovation Technology Fund (ITF) under project number ITS/369/15.

References

[1] J.C. Wataha, G. Schmalz, Dental Alloys, Biocompatibility of Dental Materials, Springer, Berlin, Heidelberg, 2009, pp. 221–254.
[2] N.J. Hallab, A. Skipor, J.J. Jacobs, Interfacial kinetics of titanium- and cobalt-based implant alloys in human serum: Metal release and biofilm formation, J. Biomed. Mater. Res. 65A (2003) 311–318.
[3] B. Henriques, D. Soares, F.S. Silva, Microstructure, hardness, corrosion resistance and porcelain shear bond strength comparison between cast and hot pressed CoCrMo alloy for metal-ceramic dental restorations, J. Mech. Behav. Biomed. 12 (2012) 83–92.
[4] D. Sun, J.A. Wharton, R.J.K. Wood, Micro- and nano-scale tribo-corrosion of cast CoCrMo, Tribol. Lett. 41 (3) (2011) 525–533.
[5] D. Sun, J.A. Wharton, R.J.K. Wood, Abrasive size and concentration effects on the tribo-corrosion of cast CoCrMo alloy in simulated body fluids discussion, Tribol. Int. 42 (11–12) (2009) 1859.
[6] D. Sun, J.A. Wharton, R.J.K. Wood, Abrasive size and concentration effects on the tribo-corrosion of cast CoCrMo alloy in simulated body fluids, Tribol. Int. 42 (11–12) (2009) 1595–1604.
[7] D. Sun, J.A. Wharton, R.J.K. Wood, Micro-abrasion-corrosion of cast CoCrMo-effects of micron and sub-micron sized abrasives, Wear 267 (1–4) (2009) 52–60.
[8] D. Sun, J.A. Wharton, R.J.K. Wood, L. Ma, W.M. Rainforth, Microabrasion-corrosion of cast CoCrMo alloy in simulated body fluids, Tribol. Int. 42 (1) (2009) 99–110.
[9] R.W.W. Hsu, C.C. Yang, C.A. Huang, Y.S. Chen, Electrochemical corrosion studies on Co–Cr–Mo implant alloy in biological solutions, Mater. Chem. Phys. 93 (2–3) (2005) 531–538.
[10] S. Hiromoto, E. Onodera, A. Chiba, K. Asami, T. Hanawa, Microstructure and corrosion behaviour in biological environments of the new forged low-Ni Co-Cr-Mo alloys, Biomaterials 26 (24) (2005) 4912–4923.
[11] M.A. Vasylyev, V.A. Tinkov, V.S. Filatova, S.M. Voloshko, P.A. Gurin, Generation of the periodic surface structures on the dental Co–Cr–Mo alloy by Nd:YAG laser in an inert atmosphere, Appl. Surf. Sci. 258 (10) (2012) 4424–4427.
[12] Hallie E. Placko, S.A. Brown, J.H. Payer, Effects of microstructure on the corrosion behavior of CoCr porous coatings on orthopedic implants, J. Biomed. Mater. Res. 39 (2) (1998) 292–299.
[13] Y.N. Petrov, G.I. Prokopenko, B.N. Mordyuk, M.A. Vasylyev, S.M. Voloshko, V.S. Skorodzievski, V.S. Filatova, Influence of microstructural modifications induced by ultrasonic impact treatment on hardening and corrosion behavior of wrought Co-Cr-Mo biomedical alloy, Mater. Sci. Eng. C Mater. Biol. Appl. 58 (2016) 1024–1035.
[14] I.M.A. Mohamed, M. Motlak, M.S. Akhtar, A.S. Yasin, M.H. El-Newehy, S.S. Al-Deyab, N.A.M. Barakat, Synthesis, characterization and performance as a counter electrode for dye-sensitized solar cells of CoCr-decorated carbon nanofibers, Ceram. Int. 42 (1) (2016) 146–153.
[15] W.S. Gora, Y. Tian, A.P. Cabo, M. Ardron, R.R.J. Maier, P. Prangnell, N.J. Weston, D.P. Hand, Enhancing surface finish of additively manufactured titanium and cobalt chrome elements using laser based finishing, Phys. Procedia 83 (2016) 258–263.
[16] A. Takaichi, T. Suyalatu, N. Nakamoto, N. Joko, Y. Nomura, S. Tsutsumi, H. Migita, S. Doi, A. Kurosu, N. Chiba, Y. Wakabayashi, T. Igarashi, Hanawa, Microstructures and mechanical properties of Co–29Cr–6Mo alloy fabricated by selective laser melting process for dental applications, J. Mech. Behav. Biomed. Mater. 21 (2013) 67–76.
[17] J. Tu, K.-F. Zhou, Z.-M. Zhou, C. Huang, H.-L. Tang, Microstructural characteristics of cobalt treated by high-speed laser surface melting under high power, Mater. Charact. 128 (2017) 63–67.
[18] B. Vandenbroucke, J.P. Kruth, Selective laser melting of biocompatible metals for rapid manufacturing of medical parts, Rapid Prototyping J. 13 (4) (2007) 196–203.
[19] J.H. Jung, H.K. Park, B.S. Lee, J. Choi, B. Seo, H.K. Kim, G.H. Kim, H.G. Kim, Study on surface shape control of pure Ti fabricated by electron beam melting using electrolytic polishing, Surf. Coat. Technol. 324 (Suppl. C) (2017) 106–110.
[20] E. Ukar, A. Lamikiz, F. Liébana, S. Martínez, I. Tabernero, An industrial approach of laser polishing with different laser sources, Mater. Sci. Eng. A 46 (7) (2015) 661–667.
[21] B. Evgeny, T. Hughes, D. Eskin, Effect of surface roughness on corrosion behaviour of low carbon steel in inhibited 4M hydrochloric acid under laminar and turbulent flow conditions, Corros. Sci. 103 (2016) 196–205.
[22] J.W. Bond, The thermodynamics of latent fingerprint corrosion of metal elements and alloys, J. Forensic Sci. 53 (6) (2008) 1344–1352.
[23] P.A. Candela, L.L.Y. Chang, Solid-solution, order-disorder, and the thermodynamics of alloy corrosion, J. Electrochem. Soc. 131 (8) (1984) C298.
[24] S. Sandor, B. Istvan, The thermodynamics of welded seams and causes of its corrosion, Korroz Figy 48 (4) (2008) 76–86.
[25] Y. Yan, A. Neville, D. Dowson, Biotribocorrosion of CoCrMo orthopaedic implant materials—assessing the formation and effect of the biofilm, Tribol. Int. 40 (10–12) (2007) 1492–1499.
[26] A. Ramirez-Ledesma, H. Lopez, J. Juarez-Islas, Evaluation of chill cast Co-Cr alloys for biomedical applications, Metals 6 (8) (2016) 188.

[27] K. Rajan, Phase transformations in a wrought Co-Cr-Mo-C alloy, Metall. Trans. A 13 (7) (1982) 1161–1166.
[28] A. Bogno, H. Nguyen-Thi, G. Reinhart, B. Billia, J. Baruchel, Growth and interaction of dendritic equiaxed grains: in situ characterization by synchrotron X-ray radiography, Acta Mater. 61 (4) (2013) 1303–1315.
[29] Y.S. Hedberg, B. Qian, Z. Shen, S. Virtanen, I. Odnevall Wallinder, In vitro biocompatibility of CoCrMo dental alloys fabricated by selective laser melting, Dent. Mater. 30 (5) (2014) 525–534.
[30] E. Bettini, T. Eriksson, M. Boström, C. Leygraf, J. Pan, Influence of metal carbides on dissolution behavior of biomedical CoCrMo alloy: SEM, TEM and AFM studies, Electrochimica Acta 56 (25) (2011) 9413–9419.
[31] E. Bettini, C. Leygraf, C. Lin, P. Liu, J. Pan, Influence of grain boundaries on dissolution behavior of a biomedical CoCrMo alloy: in-situ electrochemical-optical, AFM and SEM/TEM studies, J. Electrochem. Soc. 159 (9) (2012) C422–C427.
[32] M.A. Ashworth, A.J. Davenport, R.M. Ward, H.G.C. Hamilton, Microstructure and corrosion of Pd-modified Ti alloys produced by powder metallurgy, Corros. Sci. 52 (7) (2010) 2413–2421.
[33] Z. Pu, S. Yang, G.L. Song, O.W. Dillon, D.A. Puleo, I.S. Jawahir, Ultrafine-grained surface layer on Mg–Al–Zn alloy produced by cryogenic burnishing for enhanced corrosion resistance, Scr. Mater. 65 (6) (2011) 520–523.
[34] B.N. Mordyuk, O.P. Karasevskaya, G.I. Prokopenko, Structurally induced enhancement in corrosion resistance of Zr–2.5%Nb alloy in saline solution by applying ultrasonic impact peening, Mater. Sci. Eng., A 559 (2013) 453–461.
[35] J.B. Vander Sande, J.R. Coke, J. Wulff, A transmission electron microscopy study of the mechanisms of strengthening in heat-treated Co-Cr-Mo-C alloys, Metall. Trans. A 7 (3) (1976) 389–397.
[36] V. Hancu, R.M. Comaneanu, C. Coman, A.G. Filipescu, D.L. Ghergic, M.C. Cotrut, In vitro studies regarding the corrosion resistance of NiCr and CoCr types dental alloys, Rev. Chim. – Bucharest 65 (6) (2014) 706–709.